ACS OMEGA

http://pubs.acs.org/journal/acsodf

Article

Two Shared Icosahedral Metallacarboranes through Iron: A Joint Experimental and Theoretical Refinement of Mössbauer Spectrum in $[Fe(1,2\text{-}C_2B_9H_{11})_2]Cs$

José F. Marco, Juan Z. Dávalos-Prado, Drahomír Hnyk, Josef Holub, Ofelia B. Oña, Diego R. Alcoba, Maxime Ferrer, José Elguero, Luis Lain, Alicia Torre, and Josep M. Oliva-Enrich*

Cite This: *ACS Omega* 2023, 8, 13993−14004

Read Online

ACCESS | Metrics & More | Article Recommendations | Supporting Information

ABSTRACT: Mössbauer and X-ray photoelectron spectroscopies (XPS) are complemented with high-level quantum-chemical computations in the study of the geometric and electronic structure of the paramagnetic salt of the metallacarborane sandwich complex $[Fe(1,2\text{-}C_2B_9H_{11})_2]Cs$ = FeSanCs. Experimental ^{57}Fe isomer shifts and quadrupole splitting parameters are compared with the theoretical prediction, with good agreement. The appearance of two sets of Cs(3d) doublets in the XPS spectrum, separated by 2 eV, indicates that Cs has two different chemical environments due to ease of the $Cs^{(+)}$ cation moving around the sandwich complex with low-energy barriers, as confirmed by quantum-chemical computations. Several minimum-energy geometries of the FeSanCs structure with the corresponding energies and Mössbauer parameters are discussed, in particular the atomic charges and spin population and the surroundings of the Fe atom in the complex. The Mössbauer spectra were taken at different temperatures showing the presence of a low-spin Fe atom with $S = 1/2$ and thus confirming a paramagnetic Fe^{III} species.

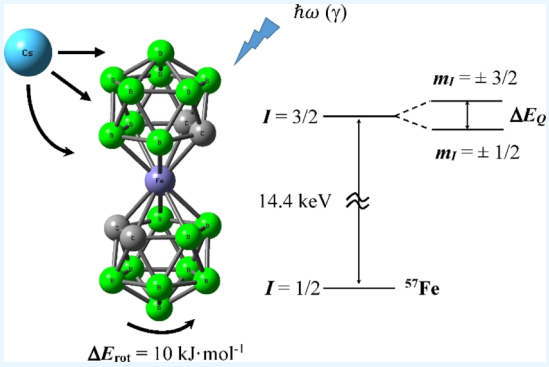

1. INTRODUCTION

Ferrocene, one of the most fruitful paradigms in organometallic chemistry,[1] represents a benchmark structure not only for a plethora of metallocenes[2] but also for the family of the so-called metallaboranes. In essence, they may be viewed as two icosahedral cages with a joint metal vertex. An archetype of these systems is obviously a hypothetical $[B_{23}H_{22}]^{2-}$ with a common naked boron atom instead of the metal.[3] Three and four naked boron atoms appear to act as joint vertices in experimentally available[4] $B_{21}H_{18}^-$ and $B_{20}H_{16}$.[5] Alternatively, two $[nido\text{-}C_2B_9H_{11}]^{(2-)}$ moieties that are similar with the cyclopentadienyl ligand, in particular, in terms of the NICS values assessing aromaticities also in individual fragments of 3D aromatic systems,[6] which confirms isolobal and isoelectronic relation of such open pentagonal belts,[7] both successfully sandwich various metal cations,[8−10] with the common labeling MSan, where M is a transition-metal atom with a given oxidation state, and "San" is an abbreviation for "Sandwich". These sandwich complexes have rich self-assembly behavior,[11] novel aromatic properties,[12] and electrochemical applications.[13]

Ferra-bis(dicarbollide) $[Fe(1,2\text{-}C_2B_9H_{11})_2]^{(-)}$, abbreviated as FeSan, has turned out to be a versatile agent in the introduction of Fe into organic molecules such as DNA dinucleotides,[14−17] in applications of medical radiotherapy,[18] as an antibacterial agent,[19] as well as an inhibitor based on formation of protein−ligand complexes.[20] Here, we should also emphasize the importance of the *closo*-dodecaborate anion $[B_{12}H_{12}]^{(2-)}$ and its applications in medicine.[21] As regards to the magnetic properties of metal centers, FeSan has also been examined in the concerted experimental/computational approach toward its paramagnetic ^{11}B spectroscopy.[22] Originally prepared diamagnetic[23] Fe^{II}San is very prone to oxidation to its paramagnetic analogue Fe^{III}San − total spin $S = 1/2$ − the latter recently proposed as a quantum bit (qubit) due to its slow-spin relaxation.[24]

On the other hand, Mössbauer spectroscopy[25] is a very useful and sensitive tool for the study of hyperfine interactions[26,27] and the elucidation of geometrical, electronic, and magnetic local environments of Mössbauer-active nuclei (here ^{57}Fe)—specifically the oxidation state of the metal center—in metal complexes and biomolecules.[28−33] The ^{57}Fe isotope is most studied in Mössbauer spectroscopy due to its very low-energy gamma-ray photon and its long-lived magnetic

Received: January 20, 2023
Accepted: March 29, 2023
Published: April 7, 2023

Downloaded via CSIC on July 12, 2023 at 07:53:52 (UTC).
See https://pubs.acs.org/sharingguidelines for options on how to legitimately share published articles.

ACS Publications

© 2023 The Authors. Published by American Chemical Society

https://doi.org/10.1021/acsomega.3c00422
ACS Omega 2023, 8, 13993−14004

excited state ($I = 3/2$). Recently developed quantum-chemical methods for the prediction of Mössbauer parameters are important complementary tools when assigning experimental signals[34−37] and predicting yet unknown complexes. Mössbauer experimental studies of ^{57}Fe carborane[38,39] complexes have been published with the first study on the FeSan anion $[^{57}Fe(1,2\text{-}C_2B_9H_{11})_2]^{(-)}$ back in 1969 by Herber.[40]

The goal of this work is to use Mössbauer and X-ray photoelectron spectroscopies (XPS), complemented with high-level quantum-chemical computations, in order to determine as accurately as possible the geometry and electronic structure of the FeSanCs system, as well as the magnetic and electric environment of the ^{57}Fe nucleus in this system, by means of measured and computed predicted isomer shifts and quadrupole splittings.

2. METHODS

2.1. Experimental Section. A sample of the cesium salt of FeSan was prepared according to the literature procedures.[8,9] The ^{57}Fe Mössbauer spectra in the transmission mode were recorded at 298.0, 77.0, and 8.6 K using a conventional constant acceleration spectrometer, a ^{57}Co(Rh) source, and a He closed-cycle cryorefrigerator. Prior to their examination, the samples were ground in an agate mortar and mixed with vacuum grease. The velocity scale was calibrated using a 6 μm thick natural iron foil. All spectra were computer-fitted, and the isomer shifts referred to the centroid of the α-Fe spectrum at room temperature.

X-ray photoelectron data were recorded using a Specs 150 electron analyzer and Al Kα radiation under vacuum better than 2×10^{-9} mbar using a constant pass energy of 100 eV for the wide-scan spectra and 20 eV for the narrow-scan spectra. The binding energy (BE) scale was referenced to the BE of the C 1s corresponding to aliphatic carbon that was set at 284.6 eV.

2.2. Quantum-Chemical Computations. Geometry optimizations and energy computations of different FeSan anions and Cs conformers in FeSanCs were carried out with the BP86 functional[41,42] and the Def2TZVP basis set,[43,44] with the scientific software Gaussian.[45] The BP86 functional, with good performance with molecular metal complex geometries,[44−46] belongs to the generalized gradient approximation (GGA) methods, where the exchange−correlation energy is a functional of the electron density $\rho(\boldsymbol{r})$ and its gradient $\nabla\rho(\boldsymbol{r})$. The Def2TZVP basis set is a valence triple-ζ with two sets of polarization functions and a set of diffuse functions.

As regards to the prediction of Mössbauer parameters, isomer shifts δ and quadrupole splittings ΔE_Q for the different geometries and Cs positions were computed with the scientific software ORCA, version 3.0.3.[47] Single-point calculations with the same BP86 functional and optimized geometries were carried out, thus obtaining the electron density values at the Fe nuclear positions that were used to derive the isomer shifts. A mixed basis set was used that consists of the core-polarized CP(PPP) basis set on Fe atoms and DKH-def2-TZVP on all other atoms. Scalar relativistic effects in the Mössbauer isomer shift calculations were accounted for using the second-order Douglas−Kroll−Hess approximation. In this work, three different calibrations were carried out[35,48−50] that have been included in Table 3.

3. RESULTS AND DISCUSSION

3.1. Mössbauer Spectroscopy. In order to put forward both experimental and computational results for scientific discussion, a brief summary of the basics behind Mössbauer spectroscopy[25,51,52] is exposed below. Mössbauer spectroscopy shows the presence of a nuclear transition, corresponding to a 14.4 keV energy photon, in the ^{57}Fe nuclei, between the states $I = 1/2$ (ground) and $I = 3/2$ (excited). We should emphasize that this spectroscopy is exquisitely sensitive to small changes in the chemical environment of Mössbauer-active nuclei, capable of detecting (energy/frequency) changes of just a few parts in 10^{11}. Mössbauer spectra are characterized by the isomer shift, δ, and the quadrupole splitting, ΔE_Q. The isomer shift accounts for the shift in the energy of the γ-ray absorption relative to a reference, usually Fe foil. The isomer shift strongly depends on the electron density at the nucleus and, consequently, it indicates changes in the bonding of the valence orbitals due to variations in covalency and 3d shielding. Hence, it has been used to evaluate oxidation and spin states as well as to determine the coordination environment of the Fe nucleus. The quadrupole splitting ΔE_Q is explained in terms of the interaction between the excited-state nuclear quadrupole moment and the electric field gradient at the nucleus; it corresponds to the energy difference between two magnetic states $m_I = \pm 3/2$ and $m_I = \pm 1/2$ in the excited nucleus with spin $I = 3/2$ and it is measured (this resonance) with Doppler effect, by means of a moving γ-ray source. The quadrupole splitting measures the nonspherical charge distribution in the excited state and turns out to be very sensitive to the coordination environment and the geometry of the complex under study. The isomer shift and the quadrupole splitting have been successfully predicted by means of density functional theory (DFT) methods. The isomer shift is related to the s electron density at the nucleus and can be evaluated according to the relation

$$\delta = \alpha(\rho_0 - C) + \beta \tag{1}$$

in which α is a constant depending on the change in the distribution of the nuclear charge upon absorption and ρ_0 means the electron density at the nucleus.[35] The constants α and β are determined by means of a linear regression analysis of the experimental isomer shifts versus the theoretically calculated electron density for a series of Fe compounds in various oxidation and spin states. These fittings must be performed for each functional and basis set employed since the electron density depends on the combination used in the calculation. Sets of calibration constants α, β, and C obtained from several methods were gathered.[53] An accuracy of better than 0.10 mm·s^{-1} (1 mm·s^{-1} = 48.075×10^{-9} eV) can usually be achieved by means of DFT methods with suitably sized basis sets. The quadrupole splitting is proportional to the largest component of the electric field gradient (EFG) tensor at the Fe nucleus and can be calculated according to

$$\Delta E_Q = \frac{1}{2} e Q V_{zz} \left(1 + \frac{\eta^2}{3}\right)^{1/2} \tag{2}$$

where e stands for the electron charge and Q means the nuclear quadrupole moment of the ^{57}Fe isotope (approximately 0.16 barns).[54] V_{xx}, V_{yy}, and V_{zz} are the electric field gradient tensor components and η is the asymmetry parameter that can be formulated as

https://doi.org/10.1021/acsomega.3c00422
ACS Omega 2023, 8, 13993−14004

$$\eta = \left| \frac{V_{xx} - V_{yy}}{V_{zz}} \right| \quad (3)$$

in a chosen coordinate system so that $|V_{zz}| \geq |V_{yy}| \geq |V_{xx}|$. Therefore, by means of quantum-chemical computations, one can obtain the electron density at the nucleus ρ_0 and the EFG components, thus obtaining predictive values of the isomer shift δ (with calibration) and the quadrupole splitting ΔE_Q, respectively. We now turn to the experiment versus theory results and discussion section for FeSanCs.

3.2. Interpretation of Experimental Results. The 298 K ^{57}Fe Mössbauer spectrum is composed of a very asymmetric doublet with an isomer shift δ = 0.17 mm s^{-1} and quadrupole splitting ΔE_Q = 1.31 mm s^{-1} (Figure 1). The spectrum recorded at room temperature at the magic angle (i.e., with the sample surface forming an angle of 54.7° with the direction of the incoming γ-ray beam) is, however, symmetric. The spectra recorded in normal incidence at lower temperatures show only slightly asymmetric doublets whose asymmetry is considerably lower than that observed at room temperature. Table 1 collects the hyperfine parameters obtained from the fit of the spectra shown in Figure 1. As expected, the isomer shift of the doublet increases with decreasing temperature due to the second-order Doppler shift, while its quadrupole splitting is nearly temperature-independent. It is also interesting to note that the linewidth becomes narrower as temperature decreases. The isomer shift and quadrupole splitting values of the doublet fall, according to the Maeda diagram,[55] within the range expected for a low-spin (S = 1/2) Fe^{III} species and correlate well with those recently reported for this compound.[56]

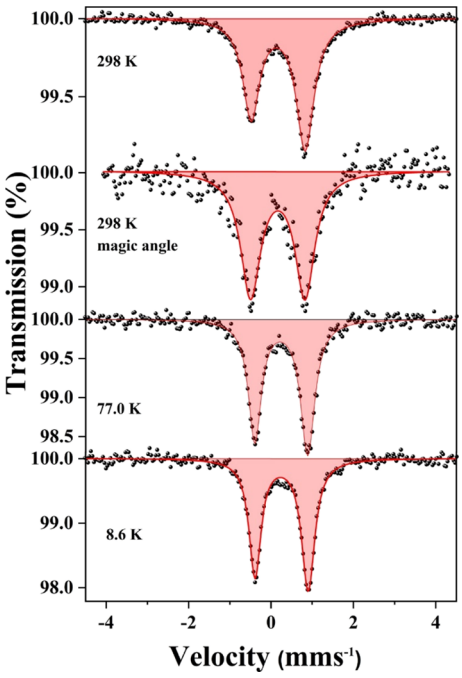

Figure 1. ^{57}Fe Mössbauer spectra recorded at different temperatures and configurations from FeSanCs.

Table 1. Mössbauer Parameters Obtained from the Fit of the Spectra Shown in Figure 1[a]

temperature and incidence angle	δ (mm s^{-1})	ΔE_Q (mm s^{-1})	Γ (mm s^{-1})	Γ_1/Γ_2	A_1/A_2
298.0 K (θ = 90°)	0.17	1.31	0.52	0.94	0.71
298.0 K (θ = 54.7°)	0.16	1.32	0.56	1.03	1.03
77.0 K (θ = 90°)	0.25	1.28	0.42	0.91	0.82
8.6 K (θ = 90°)	0.26	1.29	0.39	0.92	0.82

[a] δ = isomer shift; ΔE_Q = quadrupole splitting; Γ = fwhm; and A = area. The subindexes 1 and 2 refer to the lines 1 and 2 of the doublet, respectively.

Figure 2a depicts the wide-scan XPS spectrum recorded from the FeSanCs sample. It contains the expected C, Cs, Fe, and B contributions plus an additional oxygen contribution which is undoubtedly due to the adventitious contamination layer which is usually formed on the surface of the material which have been exposed to the atmosphere. This implies that a part of the carbon signal observed in the spectra is also due to this adventitious contamination layer.

The Cs 3d spectrum (Figure 2b) is rather complex. It is dominated by a large spin−orbit doublet Cs 3d(1) with BEs of the Cs 3d$_{5/2}$ and Cs 3d$_{3/2}$ core levels appearing at 725.1 and 739.1 eV, respectively. The spectrum also contains a minor Cs 3d doublet, Cs 3d(2), with BEs 723.0 eV (Cs 3d$_{5/2}$) and 737.0 eV (Cs 3d$_{3/2}$). On the right-hand side of the spectrum, the peak located at 721.0 eV corresponds to the Fe 2p$_{1/2}$ core level which overlaps strongly with the Cs 3d spectrum. Finally, the very small peak at 729.1 eV is the X-ray satellite of the Cs 3d$_{3/2}$ peak.

As mentioned above, the Fe 2p and Cs 3d spectra show a considerable overlap. Moreover, the X-ray satellites corresponding to the Cs 3d$_{5/2}$ peak fall in the middle of the Fe 2p spectrum. These satellites were removed using the subtraction routine available in the CasaXPS software package. Figure 2c shows the spectrum recorded along the Cs 3d$_{5/2}$ and Fe 2p spectral region once the mentioned X-ray satellites have been subtracted. We fitted the spectrum taking into account the results of fitting the Cs 3d spectrum and adding the iron contributions. The Fe 2p spectrum is composed by a quite narrow doublet [full width at half-maximum (fwhm) = 2.8 eV] with BEs of the Fe 2p$_{3/2}$ and Fe 2p$_{1/2}$ core levels of 708.5 and 720.9 eV (respectively). The spectrum also shows a small additional satellite peak at 712.1 eV whose area is about 0.16 times the area of the main Fe 2p$_{3/2}$ peak. Figure 2d shows the Fe 2p spectrum obtained from the spectrum shown in Figure 2c after subtraction of the Cs 3d$_{5/2}$ spectral features. Finally, the B 1s spectrum (not shown) is composed of a single peak located at 188.7 eV.

The Fe 2p data, both in terms of the BE of the main Fe 2p$_{3/2}$ core level, the spin−orbit splitting of ca. 12.5 eV, the fwhm of 2.8 eV, and the presence of a modest satellite 3.6 eV above the main Fe 2p$_{3/2}$ peak having an area about 0.2 times that of the latter, are all characteristic of low-spin Fe^{III} complexes.[57] These results endorse the Mössbauer results on the character of the iron species in FeSanCs.

Finally, the BE of the B 1s core level is similar to that found in related borane compounds.[58]

The room-temperature Mössbauer spectrum recorded from FeSanCs shows a very asymmetric quadrupole doublet. There are various reasons to observe an asymmetric doublet in a Mössbauer spectrum:[25] (i) the occurrence of texture, if the crystallites which compose the sample are not oriented at random; (ii) the occurrence of an anisotropic recoil free fraction, also called Goldanskii−Karyagin effect, which arises from differences in the vibrational movement of the atoms in the lattice and that, consequently, is temperature dependent;

https://doi.org/10.1021/acsomega.3c00422
ACS Omega 2023, 8, 13993−14004

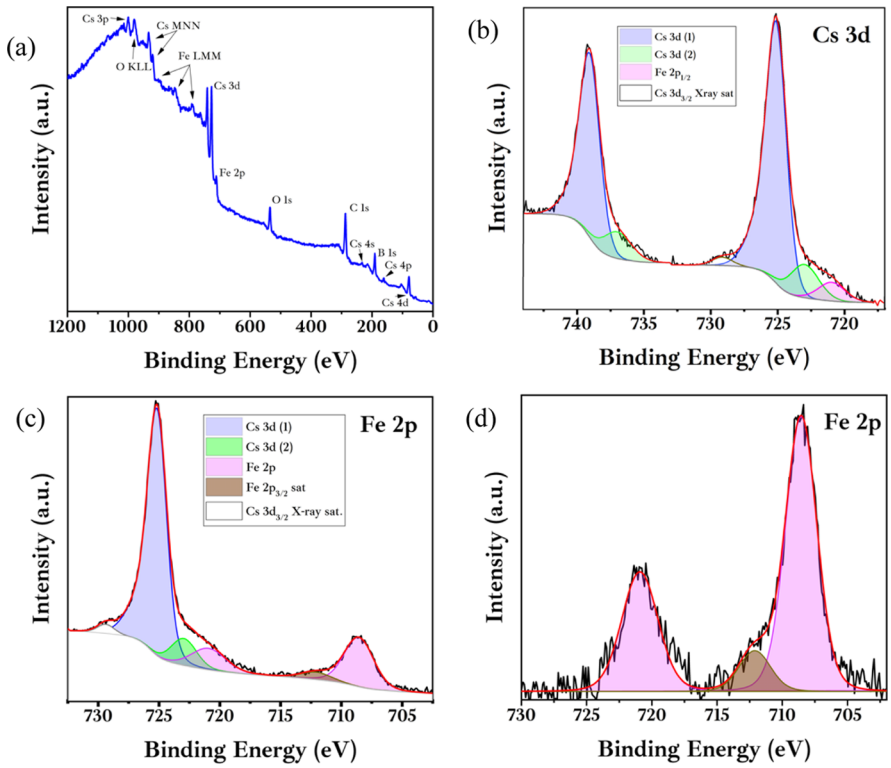

Figure 2. XPS spectra recorded for FeSanCs. (a) Wide scan; (b) Cs $3d_{3/2}$ spectrum; (c) Cs $3d_{5/2}$ and Fe 2p spectrum; and (d) Fe 2p.

(iii) the occurrence of dipolar spin−spin relaxation;[59] and (iv) the presence of several contributions to the spectrum having different isomer shifts and quadrupole splitting.

Inspection of Figure 1 and Table 1 shows that the marked asymmetry of the room-temperature spectrum disappears when the spectrum is recorded at the magic angle. This is a clear indication that the sample is textured and that its crystallites are not randomly orientated. An important point is that the spectra taken at low temperatures at normal incidence are also asymmetric, but their asymmetry is much lower than that shown by the spectrum recorded at room temperature in the same geometrical configuration. This points strongly to the concomitant occurrence of other phenomena such as the Goldanskii−Karyagin effect, that is, as explained above, of vibrational anisotropy and/or dipolar spin−spin relaxation.

The linewidth of the room-temperature spectrum is very large (0.52 mm s^{-1}). Usually, such large linewidth is an indication of the existence of structural/vibrational disorder and/or some degree of relaxation. Structural disorder, that is, the occurrence of various similar configurations having slightly different crystallographic parameters (interatomic distances or angles, for example) giving place to slightly different electric field gradient magnitudes, can be at the origin of an increased linewidth. In fact, this broadening of the spectra has been interpreted[56] as a consequence of Fe^{III} alternately jumping among three different possible geometrical configurations, each one characterized by a slightly different electric field gradient, over a characteristic Mössbauer observation time of 141 ns. At lower temperatures, the iron ion would be in the lowest energy configuration, the linewidth becoming consequently narrower.

The present Mössbauer results have shown that the quadrupole splitting of the doublet is temperature-independent as reported elsewhere.[56] This is a somehow unexpected result a priori since, in its low-spin configuration, Fe^{III} has an unpaired 3d electron; therefore, a strong thermal dependence of the population of the electronic levels, and then of the quadrupole splitting, should occur.[58] This would imply that, in the present case, the lattice contribution to the electric field gradient dominates over the valence contribution.

It is important at this point to take into account the possible geometrical configurations of the low-spin Fe^{III} ion in FeSanCs. Figure 3 shows several possible configurations. In this system, the boron atoms have practically formal 0 electric charge, (though hydrogen atoms are negatively charged), and therefore, the contributions to the lattice term of the electric field gradient would come mostly from the four carbon atoms in the vicinity of the iron ion. As the calculations have proven, the most stable configuration is that shown in Figure 3a, in which the low-spin Fe^{III} ion is in a very distorted geometry (Figure 3d). We should emphasize that the interaction of Cs with Fe is justified by the existence of a protonized FeSan.[60] In the other two less-stable configurations, the low-spin Fe^{III} ion is also distorted in a rectangular planar geometry. In the next subsection and the Supporting Information file, we describe in more detail these configurations and their energies. It would be then plausible to think that the relatively low quadrupole splitting for such iron configuration, which is nearly temperature-independent, would result from a dominant lattice contribution that overcomes, at any temperature between 298.0 and 8.6 K, the valence contribution.

The surface compositional analysis by XPS has indicated that the sample contains only the elements expected for FeSanCs, although with a small contribution due to the usual adventitious contamination layer that builds up on the surface of any material which has been produced ex situ the UHV analysis chamber and exposed to the atmosphere.

The Cs 3d spectrum contains two cesium contributions: a major one, accounting for 83% of all the cesium species, and a

https://doi.org/10.1021/acsomega.3c00422
ACS Omega 2023, 8, 13993−14004

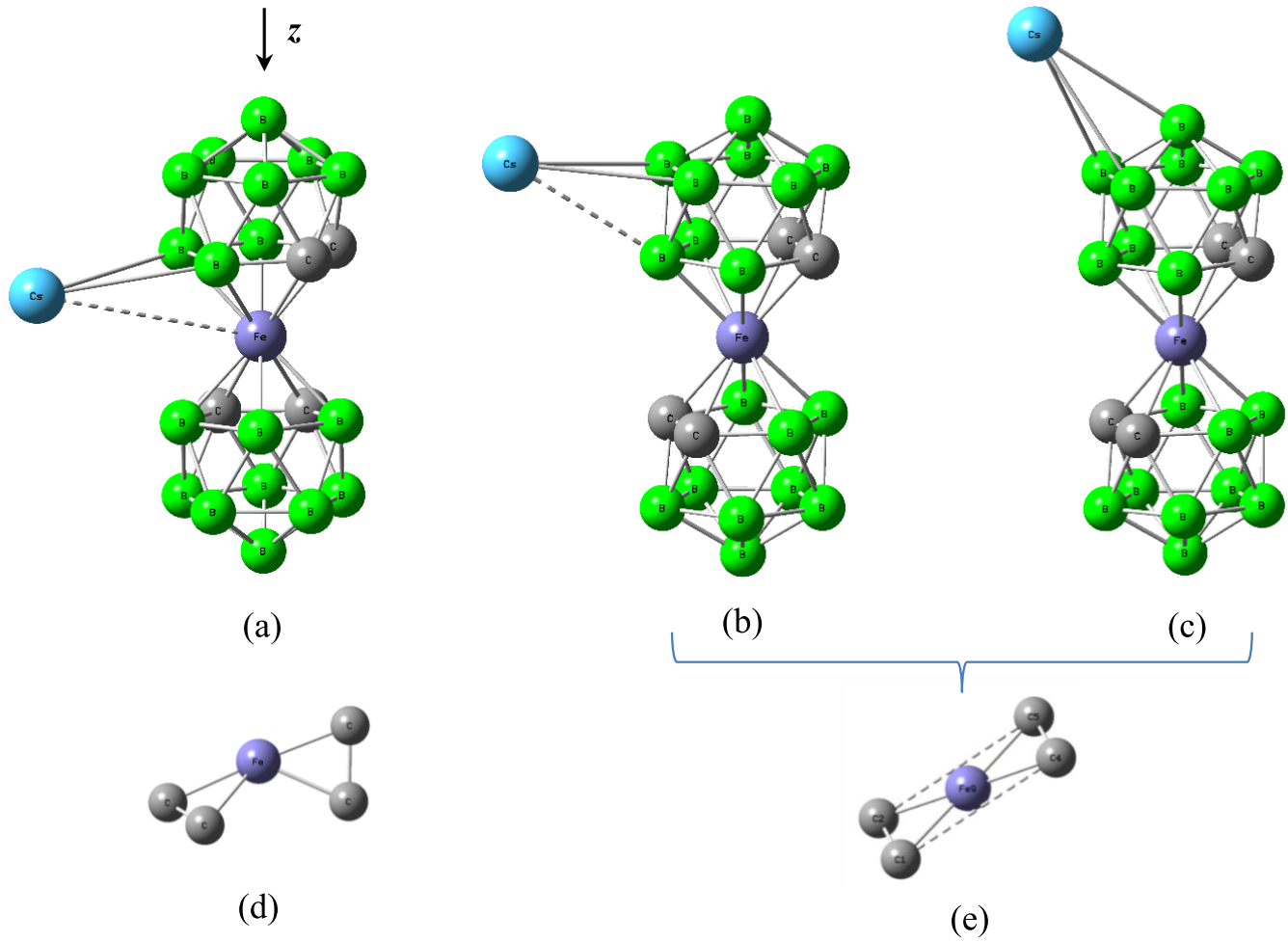

Figure 3. Selected low-energy isomers (a) ***a*** (C_1), (b) ***b*** (C_s), and (c) ***c*** (C_s) for FeSanCs. Their stability decreases in the order ***a*** > ***b*** > ***c*** as shown by quantum-chemical computations, see Table 2; (d) geometry of the iron−carbon system in isomer ***a***; and (e) geometry of the iron−carbon system in isomers ***b*** and ***c***. Isomer ***a*** differs from isomers ***b*** and ***c*** by a 72° rotation of the lower $C_2B_9H_{11}^{(2-)}$ ligand with respect to the vertical axis *z* passing through Fe and the apical boron atoms (B−Fe−B). Hydrogen atoms are not shown for clarity.

Table 2. Energy *E*(au), Gibbs Free Energy *G* (au), Energy Differences Δ*E* (kJ·mol^{-1}), and Gibbs Free Energy Differences Δ*G* (kJ·mol^{-1}) for FeSanCs Isomers *a*, *b*, and *c* from Figure 3 and FeSan Anion Conformers Trans, Intermediate (int), and Cis from Figure 4, with the Corresponding Rotational Barriers ΔE_{rot} (kJ·mol^{-1}) and ΔG_{rot} (kJ·mol^{-1})[a]

FeSanCs	NIF	PG	energy	Δ*E*	*G*	Δ*G*
a (int)	0	C_1	−1897.621102	0.0	−1897.352833	0.0
b (trans)	0	C_s	−1897.612237	23.3	−1897.343922	23.4
c (trans)	0	C_s	−1897.609860	29.5	−1897.342019	28.4

FeSan	NIF	PG	energy	Δ*E*	ΔE_{rot}	*G*	Δ*G*	ΔG_{rot}
trans	0	C_{2h}	−1877.458241	0.0		−1877.185648	0.0	
TS_3	1	C_2	−1877.454761		9.1	−1877.180969		12.3
int	0	C_2	−1877.457133	2.9		−1877.184459	3.1	
TS_2	1	C_2	−1877.451377		15.1	−1877.176674		20.4
cis	0	C_2	−1877.452468	15.2		−1877.180662	13.1	
TS_1	1	C_{2v}	−1877.447461		13.1	−1877.172768		20.7
cis'	0	C_2	−1877.452468	15.2		−1877.180662	13.1	

[a]NIF: number of imaginary frequencies of the energy minimum (NIF = 0) or transition state (NIF = 1) structures. PG: point-group symmetry.

minor one which accounts for 17% of the total cesium species. The results suggest, then, that the sample studied could contain two different FeSanCs isomers. Tentatively, we associate the major doublet with the most stable FeSanCs configuration, but we do not have enough data as to associate the second cesium species with one or other of the two possible FeSanCs configurations. It could also occur that the minor cesium contribution corresponded to a cesium-containing impurity in the sample not related to the metal carborane.

https://doi.org/10.1021/acsomega.3c00422
ACS Omega 2023, 8, 13993−14004

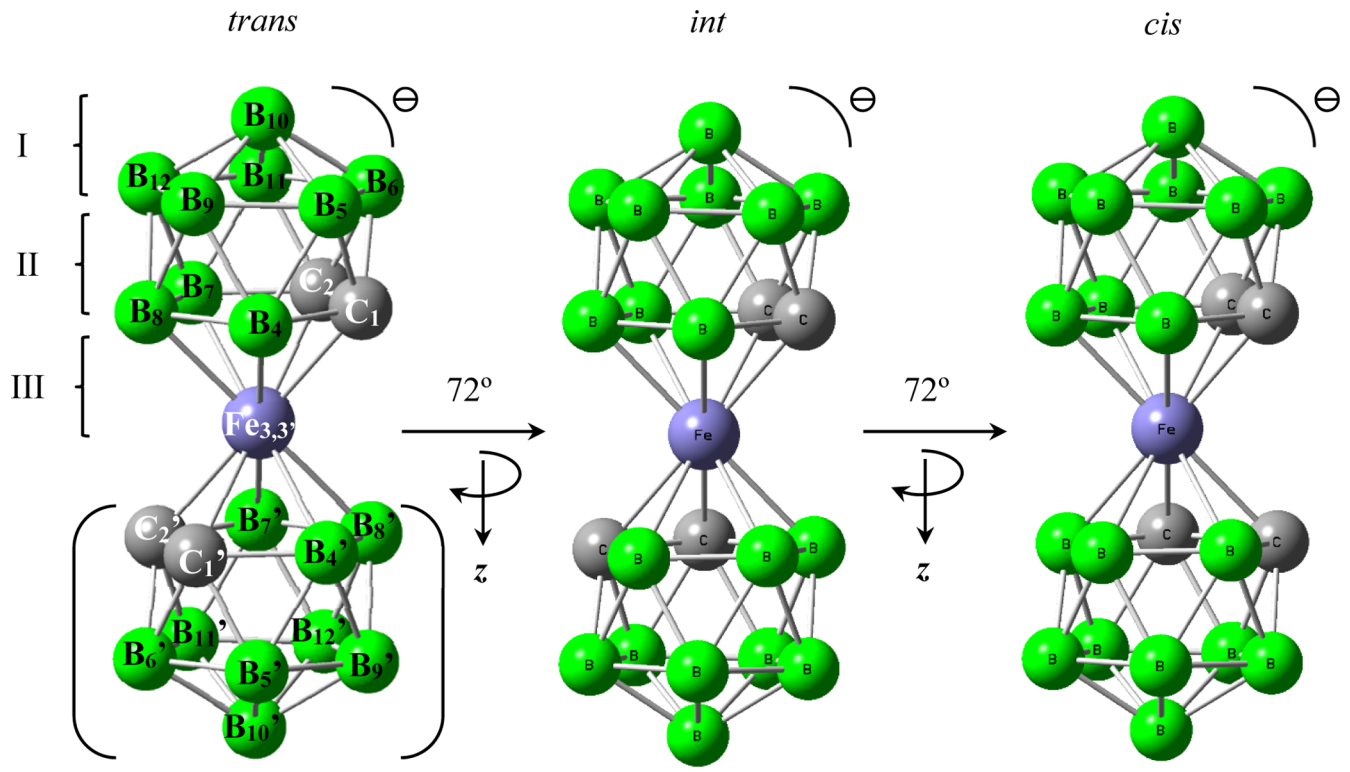

Figure 4. Trans, intermediate, and cis conformations (from left to right) in the FeSan anion, connected by consecutive 72° rotations of the lower $(C_2B_9H_{11})^{(2-)}$ moiety around the vertical *z* axis. These conformers are energy minima and have C_{2h}, C_2, and C_2 symmetry, respectively. Hydrogen atoms are removed for clarity. The meaning of areas I, II, and III in the trans conformer is explained below.

3.3. Interpretation of Theoretical Results. According to quantum-chemical computations and in agreement with previous computational studies,[22,23] the FeSan anion in the gas phase is slightly more stable in the *trans* conformation (isomers ***b*** and ***c*** from Figure 3), as compared to the *cis* conformation with the two carbon atoms from each $(C_2B_9H_{11})^{2-}$ moiety close above each other in alternate positions. The conformation with two carbon atom groups above each other—eclipsed conformation and C_{2v} symmetry—corresponds to the transition state TS_1 from Table 2, which is 13 kJ·mol^{-1} above the *cis* energy minimum, as shown in Figure 4 below. The intermediate (int) conformation in the FeSan anion corresponds to configuration ***a*** in FeSanCs in Figure 3 and a rotation of 72° of one $(C_2B_9H_{11})^{2-}$ ligand around the vertical axis with respect to the *cis* minimum. A further rotation of 72° leads to the trans conformation, which is the global energy minimum. The three energy minimum conformers in the FeSan anion are displayed in Figure 4: trans, intermediate, and cis.

The Gibbs free energy difference between the trans and intermediate (int) FeSan anion conformers is only 3.1 kJ·mol^{-1}, a value very close to $k_B \cdot T_{room}$, and the energy barrier conversion is 12.3 kJ·mol^{-1} (Table 2); therefore, at room temperature, both minima should be present. The Gibbs free energy difference between the intermediate and cis conformation is 13.1 kJ·mol^{-1}. The energy barriers for the trans → inter → cis → cis' rotational process are also gathered in Table 2, with values of 9.1, 15.1, and 13.1 kJ·mol^{-1}, respectively. The cis → cis' process corresponds to a rotation that leads to the same cis conformer (cis'), passing through TS_1, which corresponds to the C_{2v} transition state—vide supra—with the eclipsed conformation of the carbon atoms. These rotational energy barriers are very small indeed and similar to the experimental rotational barrier of ethane, ΔG_{rot} = 12 kJ·mol^{1}, between two equivalent staggered conformations and passing through the eclipsed conformation transition state.[61] The rotational Gibbs free energy barriers for the int → cis and cis → cis' rotations are both larger by ∼8 kJ·mol^{-1} respectively. Therefore, at room temperature, the three conformers should coexist, with a predominant population of trans and inter conformers, and to a lesser extent cis conformers. For example, according to the Boltzmann distribution at 298 K, the ratio trans/inter is 0.78/0.22, with the latter converted to 1 at much lower temperatures. At this point, we should take into account that the thermal energy and Gibbs free energy calculations should be taken with caution when compared to the experiment since the GGA functionals (BP86/Def2TZVP model in this work) give an agreement with experimental values within ∼8 kJ·mol^{-1}.[62] Now we turn to the electronic structure tools for elucidating the differences between conformers of the FeSan anion and isomers of the FeSanCs molecule.

We should emphasize that a recent experimental work on the same FeSanCs molecule also with ^{57}Fe Mössbauer spectroscopy has been published,[56] as mentioned above, with complementary electronic structure computations and with very similar results as compared to our experimental and quantum-chemical computations. However, in this previous published work, the different positions of the $Cs^{(+)}$ cation around the FeSan anion were not taken into account at all.

In Figure 5, the molecular electrostatic potential (MEP) $V(\boldsymbol{r})$ of the trans conformer mapped onto the 3D electron density (ρ = 0.001 au) is displayed. The MEP is a useful property for predicting anchoring points of positive and

https://doi.org/10.1021/acsomega.3c00422
ACS Omega 2023, 8, 13993−14004

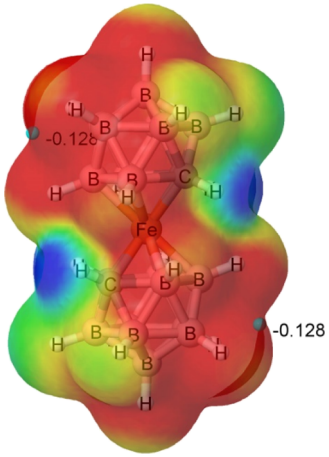

Figure 5. Molecular electrostatic potential, −0.11 (red) < $V(\boldsymbol{r})$ < −0.07 (blue), mapped onto the electron density surface with ρ = 0.001 au for the trans conformer of the FeSan anion, $[Fe^{III}(1,2\text{-}C_2B_9H_{11})_2]^{(-)}$. Red and blue areas correspond to negative (positive charge attractors) and positive (negative charge attractors) values of $V(\boldsymbol{r})$. The two equivalent MEP minima, with V = −0.128 au, are represented by gray dots.

negative charged systems onto a given molecule from an electrostatic point of view.

However, when considering FeSanCs instead of the parent FeSan anion, the energetic pattern is changed as follows. Thus, if we take the trans isomer and attach the cesium cation $Cs^{(+)}$ to the FeSan anion, many different positions correspond to energy minima: a priori above all triangular sites of one of the $(C_2B_9H_{11})^{(2-)}$ moieties, distributed into three regions, I, II, and III, as shown in Figure 4, for the trans isomer. One of the energy minima, in site II, corresponds to attaching the $Cs^{(+)}$ cation just at the MEP minimum position of Figure 5 and relaxing the geometry in order to obtain an energy minimum, leading to an optimized structure where the trans conformation of the FeSan anion is preserved. Preliminary computations with the BP86/Def2SVP model and all symmetry-unique triangular sites for each region I, II, and III and with the trans conformer (Figure 4) as initial geometries were carried out in order to select potential energy minimum geometries. Then, a geometry reoptimization with a larger basis set, Def2TZVP, and the same density hybrid functional BP86, leads to the three selected isomers displayed in Figure 3, selected as the lowest-energy isomers for each region. We should emphasize that the presence of $Cs^{(+)}$ may change the conformation of the FeSan anion during the geometry optimization process since the lowest-energy minimum isomer ***a*** in Figure 4 was initially in the trans conformation and ends up in an intermediate conformation. Hence, in isomer ***a***, the presence of the $Cs^{(+)}$ atom brings about a rotation of 72° in the lower $(C_2B_9H_{11})^{2-}$ moiety during the optimization process. Note that by changing the FeSanCs concentration, we might be able to observe rotation between trans and ***a***, which might be background for another metallacarborane rotor.[63] The relative energies of the ***a***, ***b***, and ***c*** isomers of FeSanCs and the trans, intermediate, and cis conformers of FeSan are gathered in Table 2.

As shown in Table 2, the mutual energy differences between $Cs^{(+)}$ positional conformers ***a***, ***b***, and ***c*** in FeSanCs are larger than the energy differences between the different conformers of the FeSan anion, and thus the perturbation due to the presence of $Cs^{(+)}$ is obvious. Conceivably, the Boltzmann distribution at 298 K reveals that even at 298 K, the ratios ***a***/***b*** and ***a***/***c*** is 1, that is, the cisoid conformer ***a*** strongly prevails. Such a ratio between ***b*** and ***c*** 298 K is 0.88/0.12 and results in 1 by lowering the temperatures to 77 and 8.6 K, respectively.

We now turn to the charge and spin population analysis for the different FeSan conformers and FeSanCs isomers. Since the ^{57}Fe Mössbauer nucleus is very sensitive to its electronic environment, the calculation of the atomic charges of the ligands around ^{57}Fe is relevant. Following the atom labels for the FeSan trans conformer from Figure 4, in Figure 6, the natural population charges [natural bond order (NBO)/NPA] are shown for the trans, int, and cis conformers as red and green colors for negative and positive charges, respectively. Clearly, the most negative charge is always on the Fe center, followed by the carbon atoms. The most positive charges are

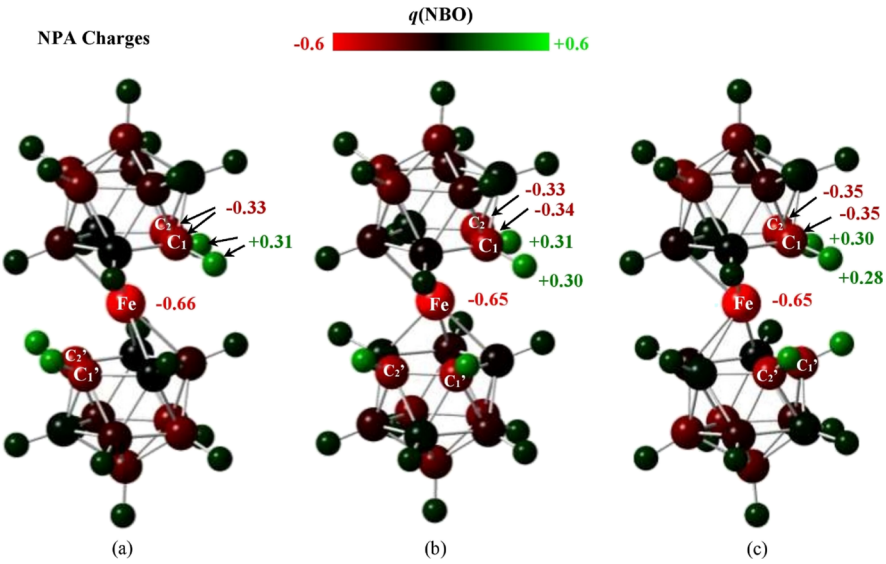

Figure 6. NBO charges q(NBO) by color for the (a) trans, (b) intermediate, and (c) cis conformers of the FeSan anion (total charge q = −1, total spin S = 1/2). BP86/Def2TZVP computations.

https://doi.org/10.1021/acsomega.3c00422
ACS Omega 2023, 8, 13993−14004

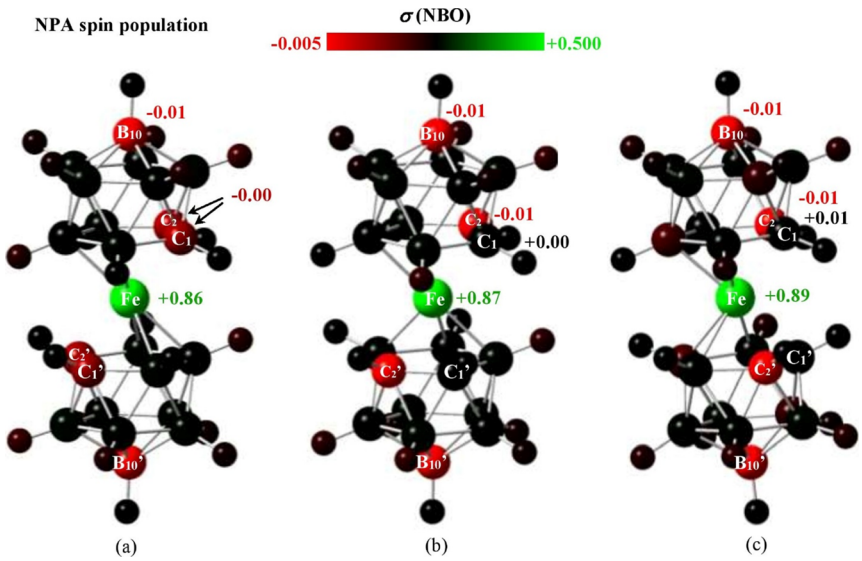

Figure 7. NBO spin population σ(NBO) by color for the (a) trans, (b) intermediate, and (c) cis conformers of the FeSan anion (total charge q = −1, total spin S = 1/2). BP86/Def2TZVP computations.

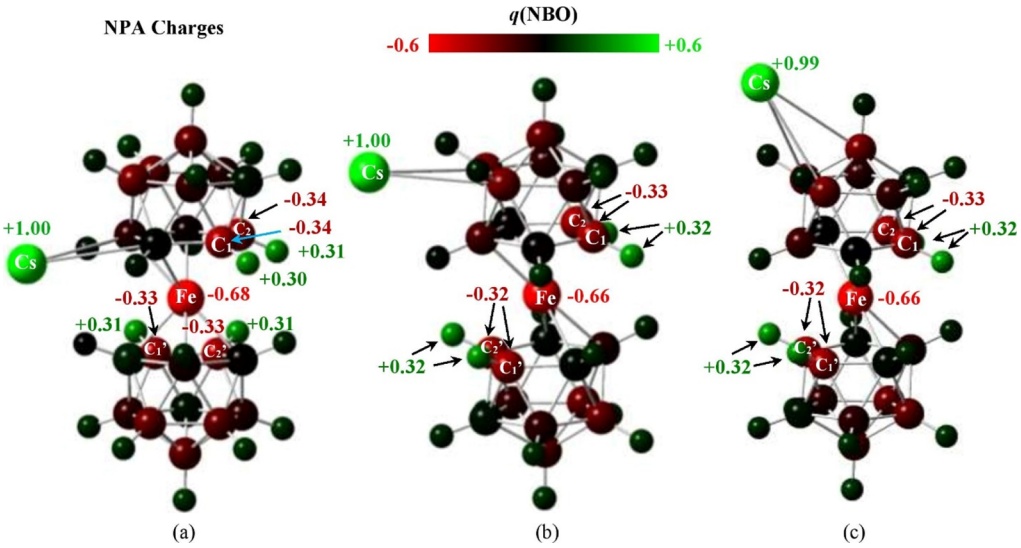

Figure 8. NBO charges q(NBO) by color for the (a) lowest-energy minimum FeSanCs isomer ***a***, (b) MEP energy minimum FeSanCs isomer ***b***, and (c) top-triangle energy minimum FeSanCs isomer ***c***. Total charge q = 0, total spin S = 1/2. BP86/Def2TZVP computations.

located on the hydrogen atoms bound to the carbon atoms. The remaining atoms have much lower negative and positive values in absolute value, which can be considered practically negligible, as shown by the very dark colors. Some boron atoms have slightly negative charges and the hydrogen atoms have slightly positive charges. In the Supporting Information file, we provide the NPA charge and spin populations for all the systems considered in this work for a full comparison. As shown in Figure 7, the highlighted NPA charges hardly change in the different conformers. When considering the S = 1/2 system, the spin population is mostly located on the Fe center, as shown in Figure 7, with other atomic centers having negligible contributions. Note that in Figure 7, the colors that represent spin populations with green and red for positive and negative spin populations are not symmetric, with a very small value (−0.005) for the negative (red) spin populations and a large value (+0.600) for the positive (green) spin populations.

We turn now to the FeSanCs conformers ***a***, ***b***, and ***c***, which correspond, respectively, to the lowest energy minimum with $Cs^{(+)}$ in position III from Figure 4, to the MEP energy minimum with $Cs^{(+)}$ in position II, and the isomer for $Cs^{(+)}$ at the top triangle area in position I. As depicted in Figure 8, the charges on the highlighted atoms are basically the same in the different isomers and compared to the charges of the three conformers from Figure 3, and the $Cs^{(+)}$ atom has practically a +1 charge in all cases. As regards to spin populations, again the Fe center has the largest and similar value in the three conformers, as shown in Figure 9. Comparison with the three conformers from Figure 9 shows that the spin populations are basically the same for all cases, and therefore, the presence of $Cs^{(+)}$ is a small perturbation in the electronic structure but a somewhat non-negligible perturbation for the geometry since the minimum-energy isomer involves an intermediate conformer with the $Cs^{(+)}$ atom close to the lower part of one of the $C_2B_9H_{11}$ ligands and the Fe center. Let us recall that the Gibbs

https://doi.org/10.1021/acsomega.3c00422
ACS Omega 2023, 8, 13993−14004

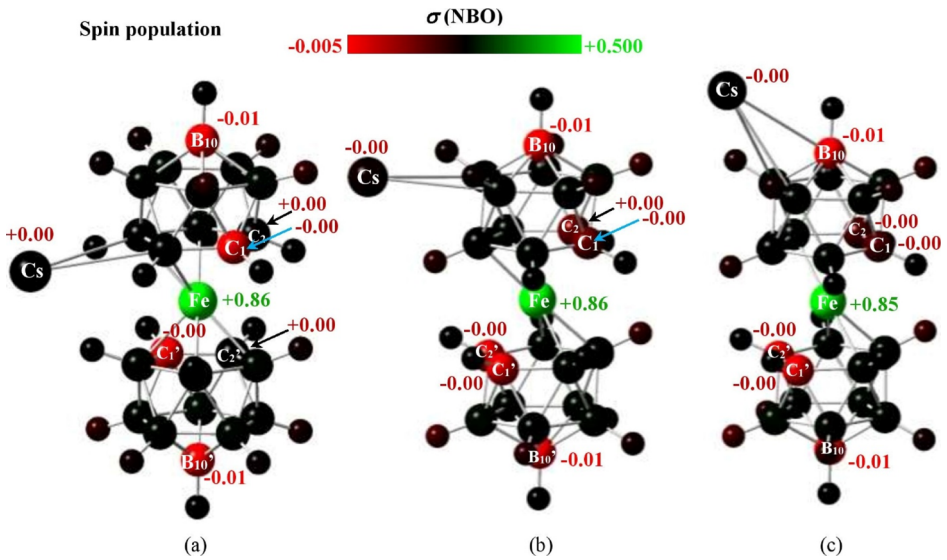

Figure 9. Natural spin populations σ(X) by color for the (a) lowest-energy minimum FeSanCs isomer ***a***, (b) MEP energy minimum FeSanCs isomer ***b***, and (c) top-triangle energy minimum FeSanCs isomer ***c***. Total charge $q = 0$, total spin $S = 1/2$. BP86/Def2TZVP computations.

Table 3. Computed Isomer Shifts δ with Three Calibrations[36] and Quadrupole Splittings ΔE_Q for the Trans, Intermediate (int), and Cis Conformers (Figure 4) of the FeSan Anion and Isomers *a*, *b*, and *c* of the FeSanCs Molecule (Figure 3)[a]

				$\delta = \alpha(\rho_0 - C) + \beta$			
system	charge	spin	ρ_0 [au^{-3}]	(i) (mm/s)	(ii) (mm/s)	(iii) (mm/s)	ΔE_Q (mm/s)
trans	−1	1/2	23661.01184	0.293	0.326	0.358	1.615
inter	−1	1/2	23661.11495	0.307	0.273	0.336	−1.432
cis	−1	1/2	23661.21867	0.254	0.287	0.314	−0.713
a	0	1/2	23661.15449	0.266	0.299	0.328	−1.440
b	0	1/2	23661.05622	0.284	0.318	0.349	1.631
c	0	1/2	23661.11300	0.274	0.307	0.337	−1.738
***T* = 9.8 K**	0	1/2		**0.26**	**0.26**	**0.26**	**1.29**

[a]Mössbauer experimental data at $T = 9.8$ K from Table 1. ρ_0 is the electron density at the nucleus. See Section 2.2 for quantum-chemical computations. (i) $\alpha = -0.187068975$; $\beta = 0.29490513$; and $C = 23661$. Calibration with a set of iron complexes with inorganic and organic ligands. (ii) $\alpha = -0.19164271$; $\beta = 0.3287136$; and $C = 23661$. The iron−sulfur molecule calibration test with experimental Mössbauer isomer shifts from refs 35 and 50. (iii) $\alpha = -0.213648857$; $\beta = 0.360662808$; and $C = 23661$. A combined test set of molecules from (i,ii). For a more detailed description of these calibrations, see Section S3 of the Supporting Information file in ref 36.

free energy difference between the trans and intermediate conformers in the FeSan anion is only 3 kJ·mol^{-1} and the Gibbs free energy barrier of rotation between them is only 12 kJ·mol^{-1}; these are small enough quantities to be overcome by the presence of a $Cs^{(+)}$ cation.

Turning now to the prediction of Mössbauer spectroscopy parameters, in Table 3, we gather computed isomer shifts δ and quadrupole splittings ΔE_Q for all the systems considered in this work, comparing them to the experimental values. In the Supporting Information file, we provide a comprehensive description of principal axes of the EFG tensors for each system.

The footnote in Table 3 describes the calibration parameters for the BP86 functional for each type of calibration used (referred to the Mössbauer calibration spectrum for α-^{57}Fe). The parameters α and β in the equation $\delta = \alpha(\rho_0 - C) + \beta$ were fitted to experimental isomer shifts and computed electron densities for molecules in three different test sets, as described in Section S3 of the Supporting Information file in ref 36. The parameter C is chosen to have approximately the same value as the calculated ρ_0 value (electron density at the nucleus) for the BP86 functional.

As shown in Table 3, the isomer shifts of the FeSan anion conformers are very similar, with a maximum difference of 0.053 mm·s^{-1}. We should emphasize that the trans → intermediate rotation in the FeSan anion involves a change in the isomer shift of only 0.014 mm·s^{-1} and that the lowest-energy conformer, trans, has an isomer shift $\delta = 0.293$ mm·s^{-1}, not very far from the experimental value. As regards to quadrupole splittings, there are remarkable changes for the different conformers, in absolute value: ΔE_Q(trans) > ΔE_Q(inter) ≫ ΔE_Q(cis), with consecutive differences of 0.183 and 0.719 mm·s^{-1}. The peculiar large differences between the values of the trans and cis isomers stem from the distribution of carbon atoms around the Fe center, which changes from a planar rectangular conformation in the trans conformer to a distorted conformation in the cis conformer; see e.g., Figure 3d,e. Let us recall that the relevant charges of the systems considered involve the Fe and C atoms, with much minor contributions from the B atoms. Clearly, the best calibration for isomer shift corresponds to (i) since it contains a set of simple iron complexes,[23] with very good agreement between isomer ***a*** (lowest energy minimum) and the experimental value. What is then the influence of attaching

https://doi.org/10.1021/acsomega.3c00422
ACS Omega 2023, 8, 13993−14004

the $Cs^{(+)}$ cation to the FeSan anion as regards to Mössbauer parameters? The presence of $Cs^{(+)}$ involves three different types of energy minimum isomers: isomer ***a*** has an intermediate conformation and both ***b*** and ***c*** isomers have a trans conformation. Clearly, the predicted isomer shift and quadrupole splitting from isomer ***a*** are in good agreement with the experimental values, with differences of 0.006 and 0.150 $mm{\cdot}s^{-1}$, respectively. Let us recall that 1 $mm{\cdot}s^{-1}$ is equivalent to 4.8×10^{-8} eV. For isomers ***b*** and ***c***, these differences increase to 0.024 (0.341) $mm{\cdot}s^{-1}$ and 0.014 (0.448) $mm{\cdot}s^{-1}$ for δ (ΔE_Q) parameters compared to the experiment.

In order to visualize the changes of the electric field as a function of structure, we have included in the Supporting Information file plots of electric field lines for the trans FeSan anion conformer (C_{2h}) and isomers ***b*** and ***c*** (C_s symmetry) of the FeSanCs molecule.[64]

4. CONCLUSIONS

In summary, the Mössbauer and XPS results confirm that iron in FeSanCs is a low-spin, (S = 1/2) Fe^{III} species. The Mössbauer data have shown the occurrence of both texture effects and vibrational disorder/spin−spin relaxation in the solid, all facts probably related to the distorted geometrical configuration of the Cs−C system, given the low-energy barriers to rotation of the $(C_2B_9H_{11})^{(2-)}$ ligands around the B_{10}−Fe^{III}−B_{10}' vertical axis in the FeSan anion and the structural perturbations due to the presence of the large $Cs^{(+)}$ cation. The Cs 3d spectra suggest the presence of two different cesium species, which could be probably related to the existence of two different FeSanCs conformers in the sample. In any case, this appears not to affect the Mössbauer spectra except from being responsible of a fraction of the mentioned broadness of the spectral linewidths. The lowest-energy isomer of the FeSanCs molecule results in the Cs cation located approximately in a lower triangle of one of the $C_2B_9H_{11}$ ligands and "close" to the Fe center. In this structure, the FeSan anion corresponds to an intermediate conformer between the trans and cis systems; this is not a surprise given the very low energy difference (3 $kJ{\cdot}mol^{-1}$) computed between the trans and intermediate conformers of the FeSan anion and the low-energy barriers to rotation. The charge and spin population of the FeSan anion and FeSanCs molecule shows similar data regardless of the Cs position and conformer; the main differences stem from the Fe and C centers of the systems. As regards to the computed Mössbauer parameters, the isomer shift and quadrupole splitting values are close to the experimental values if we take the intermediate conformers of the FeSan anion and the lowest-energy ***a*** isomer of the FeSanCs salt. We hope that the experimental and theoretical results presented here can throw more light onto the interpretation of Mössbauer spectroscopy of metallaheteroborane compounds.

■ ASSOCIATED CONTENT

Supporting Information

The Supporting Information is available free of charge at https://pubs.acs.org/doi/10.1021/acsomega.3c00422.

Cartesian coordinates of the optimized geometries in the stationary points (energy minima and transition states) of the systems included in this work; charge and spin populations for the energy minima systems included in this work; principal axes and eigenvalues of the electric field gradient matrix of the energy minima conformers included in this work; electric field lines for the trans conformer of the FeSan anion and ***b*** and ***c*** isomers of the FeSanCs molecule; and XPS spectrum of the boron 1*s* energy levels in the $[Fe(1,2\text{-}C_2B_9H_{11})_2]Cs$ sample (PDF)

■ AUTHOR INFORMATION

Corresponding Author

Josep M. Oliva-Enrich − *Instituto de Química-Física "Rocasolano", CSIC, E-28006 Madrid, Spain;* orcid.org/0000-0001-9108-8615; Email: j.m.oliva@iqfr.csic.es

Authors

José F. Marco − *Instituto de Química-Física "Rocasolano", CSIC, E-28006 Madrid, Spain*

Juan Z. Dávalos-Prado − *Instituto de Química-Física "Rocasolano", CSIC, E-28006 Madrid, Spain;* orcid.org/0000-0002-5835-6371

Drahomír Hnyk − *Institute of Inorganic Chemistry of the Czech Academy of Sciences, CZ-250 68 Řež near Prague, Czech Republic;* orcid.org/0000-0001-8094-7509

Josef Holub − *Institute of Inorganic Chemistry of the Czech Academy of Sciences, CZ-250 68 Řež near Prague, Czech Republic*

Ofelia B. Oña − *Instituto de Investigaciones Fisicoquímicas Teóricas y Aplicadas, Universidad Nacional de La Plata, CCT La Plata, Consejo Nacional de Investigaciones Científicas y Técnicas, 1900 La Plata, Argentina*

Diego R. Alcoba − *Departamento de Física, Facultad de Ciencias Exactas y Naturales, Universidad de Buenos Aires, Ciudad Universitaria, 1428 Buenos Aires, Argentina; Instituto de Física de Buenos Aires, Consejo Nacional de Investigaciones Científicas y Técnicas, Ciudad Universitaria, 1428 Buenos Aires, Argentina*

Maxime Ferrer − *Instituto de Química Médica, CSIC, E-28006 Madrid, Spain; Theoretical Chemistry and Computational Modelling, Doctoral School, Universidad Autónoma de Madrid, 28049 Madrid, Spain*

José Elguero − *Instituto de Química Médica, CSIC, E-28006 Madrid, Spain;* orcid.org/0000-0002-9213-6858

Luis Lain − *Departamento de Química Física, Facultad de Ciencia y Tecnología, Universidad del País Vasco, E-48080 Bilbao, Spain;* orcid.org/0000-0002-7260-049X

Alicia Torre − *Departamento de Química Física, Facultad de Ciencia y Tecnología, Universidad del País Vasco, E-48080 Bilbao, Spain*

Complete contact information is available at: https://pubs.acs.org/10.1021/acsomega.3c00422

Notes

The authors declare no competing financial interest.

■ ACKNOWLEDGMENTS

We are grateful to Prof. Ibon Alkorta (IQM-CSIC) for providing the MEP of trans-FeSan anion conformer. J.F.M. and J.Z.D.-P. acknowledge financial support from grant RTI2018-095303-B-C51 funded by MCIN/AEI/10.13039/501100011033 and by "ERDF A way of making Europe" and from grant S2018-NMT-4321 funded by the Comunidad de Madrid and by "ERDF A way of making Europe". M.F., J.E., and J.M.O.-E. are grateful to Ministerio de Ciencia, Innovación

y Universidades, for financial support with grant number PID2021-125207NB-C32. O.B.O. and D.R.A. acknowledge the financial support from the Universidad de Buenos Aires (grant no. 20020190100214BA), the Consejo Nacional de Investigaciones Científicas y Técnicas (grant nos PIP 11220200100467CO, PIP 11220130100377CO, and PIP 11220130100311CO), and the Agencia Nacional de Promoción Científica y Tecnológica, Argentina (grant no. PICT-2010381).

REFERENCES

(1) Adams, R. D. Foreword. *J. Organomet. Chem.* **2001**, *637−639*, 1.

(2) Haaland, A. Molecular structure and bonding in the 3d metallocenes. *Acc. Chem. Res.* **1979**, *12*, 415−422.

(3) Hnyk, D.; Holub, J.; Jelínek, T.; Macháček, J.; Londesborough, M. G. S. Revisiting $B_{20}H_{16}$ by means of a joint computational/experimental NMR approach. *Collect. Czech. Chem. Commun.* **2010**, *75*, 1115−1123.

(4) (a) Eyrilmez, S. M.; Bernhardt, E.; Dávalos, J. Z.; Lepšík, M.; Hobza, P.; Assaf, K. I.; Nau, W.; Holub, J.; Oliva-Enrich, J. M.; Fanfrlík, J.; Hnyk, D. Binary twinned-icosahedral $[B_{21}H_{18}]^-$ interacts with cyclodextrins as a precedent for its complexation with other organic motifs. *Phys. Chem. Chem. Phys.* **2017**, *19*, 11748−11752. (b) Assaf, K.; Holub, J.; Bernhardt, E.; Oliva-Enrich, J. M.; Fernández Pérez, M. I.; Canle, M.; Santaballa, J. A.; Fanfrlík, J.; Hnyk, D.; Nau, W. Face-fusion of icosahedral boron hydride increases affinity to γ-cyclodextrin: closo,closo-$[B_{21}H_{18}]^-$ as an anion with very low free energy of dehydration. *ChemPhysChem* **2020**, *21*, 971−976.

(5) Dobrott, R. D.; Friedman, L. B.; Lipscomb, W. N. Molecular and crystal structure of $B_{20}H_{16}$. *J. Chem. Phys.* **1964**, *40*, 866−872.

(6) Schleyer, P. v. R.; Maerker, Ch.; Dransfeld, A.; Jiao, H.; van Eikema Hommes, N. J. R. Nucleus-independent chemical shifts: a simple and efficient aromaticity probe. *J. Am. Chem. Soc.* **1996**, *118*, 6317−6318.

(7) Holub, J.; Melichar, P.; Růžičková, Z.; Vrána, J.; Wann, D. A.; Fanfrlík, J.; Hnyk, D.; Růžička, A. A novel stibacarbaborane cluster with adjacent antimony atoms exhibiting unique pnictogen bond formation that dominates its crystal packing. *Dalton Trans.* **2017**, *46*, 13714−13719.

(8) Hawthorne, M. F.; Young, D. C.; Wegner, P. A. Carbametallic Boron Hydride Derivatives. I. Apparent analogs of ferrocene and ferricinium ion. *J. Am. Chem. Soc.* **1965**, *87*, 1818−1819.

(9) Hawthorne, M. F.; Andrews, T. D. Carborane analogues of cobalticinium ion. *Chem. Commun.* **1965**, 443−444.

(10) Werner, H. At least 60 years of ferrocene: the discovery and rediscovery of the sandwich complexes. *Angew. Chem., Int. Ed.* **2012**, *51*, 6052−6058.

(11) Malaspina, D. C.; Vinas, C.; Teixidor, F.; Faraudo, J. Atomistic simulations of COSAN: amphiphiles without a head-and-tail design display "head and tail" surfactant behavior. *Angew. Chem., Int. Ed.* **2020**, *59*, 3088−3092.

(12) Poater, J.; Viñas, C.; Bennour, I.; Escayola, S.; Solà, M.; Teixidor, F. Too Persistent to give up: aromaticity in boron clusters survives radical structural changes. *J. Am. Chem. Soc.* **2020**, *142*, 9396−9407.

(13) Xavier, J. A. M.; Viñas, C.; Lorenzo, E.; García-Mendiola, T.; Teixidor, F. Potential application of metallacarboranes as an internal reference: an electrochemical comparative study to ferrocene. *Chem. Commun.* **2022**, *58*, 4196−4199.

(14) (a) Olejniczak, A. B.; Mucha, P.; Grüner, B.; Lesnikowski, Z. J. DNA-dinucleotides bearing a 3′,3′-cobalt- or 3′,3′-iron-1,2,1′,2′-dicarbollide complex. *Organometallics* **2007**, *26*, 3272−3274. (b) Wojtczak, B. J.; Andrysiak, A.; Grüner, B.; Lesnikowski, Z. J. Chemical ligation": a versatile method for nucleoside modification with boron clusters. *Chem.—Eur. J.* **2008**, *14*, 10675−10682.

(15) Lesnikowski, Z. J. Boron units as pharmacophores - new applications and opportunities of boron cluster chemistry. *Collect. Czech. Chem. Commun.* **2007**, *72*, 1646−1658.

(16) García-Mendiola, T.; Bayon-Pizarro, V.; Zaulet, A.; Fuentes, I.; Pariente, F.; Teixidor, F.; Viñas, C.; Lorenzo, E. Metallacarboranes as tunable redox potential electrochemical indicators for screening of gene mutation. *Chem. Sci.* **2016**, *7*, 5786−5797.

(17) Kodr, D.; Yenice, C. P.; Simonova, A.; Saftić, D. P.; Pohl, R.; Sýkorová, V.; Ortiz, M.; Havran, L.; Fojta, M.; Lesnikowski, Z. J.; O'Sullivan, C. K.; et al. Carborane- or Metallacarborane-Linked Nucleotides for Redox Labeling. Orthogonal Multipotential Coding of all Four DNA Bases for Electrochemical Analysis and Sequencing. *J. Am. Chem. Soc.* **2021**, *143*, 7124−7134.

(18) Buades, A. B.; Pereira, L. C. J.; Vieira, B. J. C.; Cerdeira, A. C.; Waerenborgh, J. C.; Pinheiro, T.; Matos, A. P. A.; Pinto, C. G.; Guerreiro, J. F.; Mendes, F.; Valic, S.; Teixidor, F.; Viñas, C.; Marques, F. The Mössbauer effect using ^{57}Fe-ferrabisdicarbollide ($[o\text{-}^{57}FeSan]^-$): a glance into the potential of a low-dose approach for glioblastoma radiotherapy. *Inorg. Chem. Front.* **2022**, *9*, 1490−1503.

(19) Bennour, I.; Ramos, M. N.; Nuez-Martínez, M.; Xavier, J. A. M.; Buades, A. B.; Sillanpää, R.; Teixidor, F.; Choquesillo-Lazarte, D.; Romero, I.; Martínez-Medina, M.; Viñas, C. Water soluble organometallic small molecules as promising antibacterial agents: synthesis, physical−chemical properties and biological evaluation to tackle bacterial infections. *Dalton Trans.* **2022**, *51*, 7188−7209.

(20) Srb, P.; Svoboda, M.; Benda, L.; Lepšík, M.; Tarábek, J.; Šícha, V.; Grüner, B.; Grantz-Šašková, K.; Brynda, J.; Řezáčová, P.; Konvalinka, J.; Veverka, V. Capturing a dynamically interacting inhibitor by paramagnetic NMR spectroscopy. *Phys. Chem. Chem. Phys.* **2019**, *21*, 5661−5673.

(21) Sivaev, I. B.; Bregadze, V. I.; Kuznetsov, N. T. Derivatives of the closo-dodecaborate anion and their application in medicine. *Russ. Chem. Bull.* **2002**, *51*, 1362−1374.

(22) Pennanen, T. O.; Macháček, J.; Taubert, S.; Vaara, J.; Hnyk, D. Ferrocene-like iron bis(dicarbollide), $[3\text{-}Fe^{III}\text{-}(1,2\text{-}C_2B_9H_{11})_2]^-$. The first experimental and theoretical refinement of a paramagnetic ^{11}B NMR spectrum. *Phys. Chem. Chem. Phys.* **2010**, *12*, 7018−7025.

(23) Bühl, M.; Holub, J.; Hnyk, D.; Macháček, J. Computational studies of structures and properties of metallaboranes. 2. Transition-metal dicarbollide complexes. *Organometallics* **2006**, *25*, 2173−2181.

(24) Buades, A. B.; Arderiu, V. S.; Maxwell, L.; Amoza, M.; Choquesillo-Lazarte, D.; Aliaga-Alcalde, N.; Viñas, C.; Teixidor, F.; Ruiz, E. Slow-spin relaxation of a low-spin S = 1/2 Fe^{III} carborane complex. *Chem. Commun.* **2019**, *55*, 3825−3828.

(25) Bancroft, G. M. *Mössbauer Spectroscopy: An Introduction for Inorganic Chemists and Geochemists*; McGraw-Hill: Maidenhead, UK, 1973.

(26) Dann, S. E.; Neumann, K. U.; Marco, J. F. Mössbauer characterisation of synthetic analogues of the helvite minerals $Fe_4M_4[BeSiO_4]_6X_2$ (M = Fe, Mn, Zn; X = S, Se). *Hyperfine Interact.* **2018**, *239*, 28.

(27) Klingelhöfer, G. Mössbauer in situ studies of the surface of mars. *Hyperfine Interact.* **2004**, *158*, 117−124.

(28) Auerbach, H.; Giammanco, G. E.; Schünemann, V. A.; Ostrowski, D.; Carrano, C. J. Mössbauer spectroscopic characterization of iron(III)−polysaccharide coordination complexes: photochemistry, biological, and photoresponsive materials implications. *Inorg. Chem.* **2017**, *56*, 11524−11531.

(29) Kuzmann, E.; Homonnay, Z.; Klencsár, Z.; Szalay, R. ^{57}Fe Mössbauer spectroscopy as a tool for study of spin states and magnetic interactions in inorganic chemistry. *Molecules* **2021**, *26*, 1062.

(30) Schünemann, V.; Winkler, H. Structure and dynamics of biomolecules studied by Mössbauer spectroscopy. *Rep. Prog. Phys.* **2000**, *63*, 263−353.

(31) Yoo, S. J.; Angove, H. C.; Papaefthymiou, V.; Burgess, B. K.; Münck, E. Mössbauer study of the MoFe protein of nitrogenase from azotobacter vinelandii using selective ^{57}Fe enrichment of the M-centers. *J. Am. Chem. Soc.* **2000**, *122*, 4926−4936.

(32) Van Stappen, C.; Decamps, L.; Cutsail, G. E., III; Bjornsson, R.; Henthorn, J. T.; Birrell, J. A.; DeBeer, S. The spectroscopy of nitrogenases. *Chem. Rev.* **2020**, *120*, 5005−5081.

https://doi.org/10.1021/acsomega.3c00422
ACS Omega 2023, 8, 13993−14004

(33) Pandelia, M.-E.; Lanz, N. D.; Booker, S. J.; Krebs, C. Mössbauer spectroscopy of Fe/S proteins. *Biochim. Biophys. Acta Mol. Cell* **2015**, *1853*, 1395−1405.
(34) McWilliams, S. F.; Brennan-Wydra, E.; MacLeod, K. C.; Holland, P. L. Density functional calculations for prediction of ^{57}Fe Mössbauer isomer shifts and quadrupole splittings in β-diketiminate complexes. *ACS Omega* **2017**, *2*, 2594−2606.
(35) Neese, F. Prediction and interpretation of the ^{57}Fe isomer shift in Mössbauer spectra by density functional theory. *Inorg. Chim. Acta* **2002**, *337*, 181−192.
(36) Bjornsson, R.; Neese, F.; DeBeer, S. Revisiting the Mössbauer isomer shifts of the FeMoco cluster of nitrogenase and the cofactor charge. *Inorg. Chem.* **2017**, *56*, 1470−1477.
(37) Young, R. D.; Frauenfelder, H.; Fenimore, P. W. Mössbauer Effect in Proteins. *Phys. Rev. Lett.* **2011**, *107*, 158102.
(38) Kudinov, A. R.; Zanello, P.; Herber, R. H.; Loginov, D. A.; Vinogradov, M. M.; Vologzhanina, A. V.; Starikova, Z. A.; Corsini, M.; Giorgi, G.; Nowik, I. Ferracarborane benzene complexes $[(\eta\text{-9-L-7,8-}C_2B_9H_{10})Fe(\eta\text{-}C_6H_6)]^+$ (L = SMe_2, NMe_3): synthesis, reactivity, electrochemistry, Mössbauer effect studies, and bonding. *Organometallics* **2010**, *29*, 2260−2271.
(39) Kudinov, A. R.; Herber, R. H.; Zanello, P.; Perekalin, D. S.; Glukhov, I. V.; Nowik, I.; Corsini, M.; Fedi, S.; Laschi, F. Synthesis, structure, electrochemistry, and mössbauer effect studies of the ferraphosphadicarbollides $[(C_5R_5)Fe(PC_2B_8H_{10})]$ (R = H, Me). *Eur. J. Inorg. Chem.* **2007**, *2007*, 4190−4196.
(40) Herber, R. H. Mössbauer spectroscopy of organometallic compounds: $Fe(C_2B_9H_{11})^{2-}$ and $(\pi\text{-}C_5H_5)Fe(C_2B_9H_{11})$. *Inorg. Chem.* **1969**, *8*, 174−176.
(41) Becke, A. D. Density-functional exchange-energy approximation with correct asymptotic behavior. *Phys. Rev. A: At., Mol., Opt. Phys.* **1988**, *38*, 3098−3100.
(42) Perdew, J. P. Density-functional approximation for the correlation energy of the inhomogeneous electron gas. *Phys. Rev. B: Condens. Matter Mater. Phys.* **1986**, *33*, 8822−8824.
(43) Weigend, F. Accurate coulomb-fitting basis sets for H to Rn. *Phys. Chem. Chem. Phys.* **2006**, *8*, 1057−1065.
(44) Weigend, F.; Ahlrichs, R. Balanced basis sets of split valence, triple zeta valence and quadruple zeta valence quality for H to Rn: design and assessment of accuracy. *Phys. Chem. Chem. Phys.* **2005**, *7*, 3297−3305.
(45) Frisch, M. J.; Trucks, G. W.; Schlegel, H. B.; Scuseria, G. E.; Robb, M. A.; Cheeseman, J. R.; Scalmani, G.; Barone, V.; Petersson, G. A.; Nakatsuji, H.; Li, X.; Caricato, M.; Marenich, A. V.; Bloino, J.; Janesko, B. G.; Gomperts, R.; Mennucci, B.; Hratchian, H. P.; Ortiz, J. V.; Izmaylov, A. F.; Sonnenberg, J. L.; Williams-Young, D.; Ding, F.; Lipparini, F.; Egidi, F.; Goings, J.; Peng, B.; Petrone, A.; Henderson, T.; Ranasinghe, D.; Zakrzewski, V. G.; Gao, J.; Rega, N.; Zheng, G.; Liang, W.; Hada, M.; Ehara, M.; Toyota, K.; Fukuda, R.; Hasegawa, J.; Ishida, M.; Nakajima, T.; Honda, Y.; Kitao, O.; Nakai, H.; Vreven, T.; Throssell, K.; Montgomery, J. A., Jr.; Peralta, J. E.; Ogliaro, F.; Bearpark, M. J.; Heyd, J. J.; Brothers, E. N.; Kudin, K. N.; Staroverov, V. N.; Keith, T. A.; Kobayashi, R.; Normand, J.; Raghavachari, K.; Rendell, A. P.; Burant, J. C.; Iyengar, S. S.; Tomasi, J.; Cossi, M.; Millam, J. M.; Klene, M.; Adamo, C.; Cammi, R.; Ochterski, J. W.; Martin, R. L.; Morokuma, K.; Farkas, O.; Foresman, J. B.; Fox, D. J. *Gaussian 16*. Revision C.01; Gaussian, Inc.: Wallingford CT, 2016.
(46) Jensen, K. P.; Roos, B. O.; Ryde, U. Performance of density functionals for first row transition metal systems. *J. Chem. Phys.* **2007**, *126*, 014103.
(47) Neese, F. The ORCA program system. *Wiley Interdiscip. Rev.: Comput. Mol. Sci.* **2012**, *2*, 73−78.
(48) Sinnecker, S.; Slep, L. D.; Bill, E.; Neese, F. Performance of nonrelativistic and quasi-relativistic hybrid DFT for the prediction of electric and magnetic hyperfine parameters in ^{57}Fe Mössbauer spectra. *Inorg. Chem.* **2005**, *44*, 2245−2254.
(49) Sandala, G. M.; Hopmann, K. H.; Ghosh, A.; Noodleman, L. Calibration of DFT functionals for the prediction of ^{57}Fe Mössbauer spectral parameters in iron−nitrosyl and iron−sulfur complexes: accurate geometries prove essential. *J. Chem. Theory Comput.* **2011**, *7*, 3232−3247.
(50) Harris, T. V.; Szilagyi, R. K. Comparative assessment of the composition and charge state of nitrogenase FeMo-cofactor. *Inorg. Chem.* **2011**, *50*, 4811−4824.
(51) Greenwood, N. N.; Gibb, T. C. *Mössbauer Spectroscopy*; Chapman and Hall: London, 1971.
(52) Fackler, J. P., Jr. *Modern Inorganic Chemistry*; Long, G. J., Ed.; *Mössbauer Spectroscopy Applied to Inorganic Chemistry*; Plenum Press: NY, 1984; Vol. *1*.
(53) Römelt, M.; Ye, S.; Neese, F. Calibration of modern density functional theory methods for the prediction of ^{57}Fe Mössbauer isomer shifts: Meta-GGA and double-hybrid functionals. *Inorg. Chem.* **2009**, *48*, 784−785.
(54) Dufek, P.; Blaha, P.; Schwarz, K. Determination of the nuclear quadrupole moment of ^{57}Fe. *Phys. Rev. Lett.* **1995**, *75*, 3545−3548.
(55) Maeda, Y. Mössbauer studies on the iron-ligand binding in hemoproteins and their related compounds. *J. Phys. Colloq.* **1979**, *40*, C2-514−C2-522.
(56) Bednarska-Szczepaniak, K.; Dziedzic-Kocurek, K.; Przelazły, E.; Stanek, J.; Leśnikowski, Z. J. Intramolecular rotations and electronic states of iron in the iron bis(dicarbollide) complex $Fe[(C_2B_9H_{11})_2]$ studied by a ^{57}Fe nuclear probe and computational methods. *Chem. Commun.* **2022**, *58*, 391−394.
(57) Brant, P.; Feltham, R. D. X-ray photoelectron spectra of iron complexes: correlation of iron 2p satellite intensity with complex spin state. *J. Electron Spectrosc. Relat. Phenom.* **1983**, *32*, 205−221.
(58) Kahlert, J. U.; Rawal, A.; Hook, J. M.; Rendina, L. M.; Choucair, M. Carborane functionalization of the aromatic network in chemically-synthesized Graphene. *Chem. Commun.* **2014**, *50*, 11332−11334.
(59) Kramm, U. I.; Ni, L.; Wagner, S. ^{57}Fe Mössbauer spectroscopy characterization of electrocatalysts. *Adv. Mater.* **2019**, *31*, 1805623.
(60) Bühl, M.; Hnyk, D.; Macháček, J. Computational studies of structures and properties of metallaboranes. Part 3: protonated iron bis(dicarbollide), $[3\text{-Fe-}(1,2\text{-}C_2B_9H_{11})_2H]^-$. *Inorg. Chem.* **2007**, *46*, 1771−1777.
(61) Kemp, J. D.; Pitzer, K. S. Hindered rotation of the methyl groups in ethane. *J. Chem. Phys.* **1936**, *4*, 749.
(62) Bursch, M.; Mewes, J.-M.; Hansen, A.; Grimme, S. Best-practice DFT protocols for basic molecular computational chemistry. *Angew. Chem.* **2022**, *134*, No. e202205735.
(63) Hawthorne, M. F.; Zink, J. I.; Skelton, J. M.; Bayer, M. J.; Liu, Ch.; Livshits, E.; Baer, R.; Neuhauser, D. Electrical or Photocontrol of the Rotary Motion of a Metallacarborane. *Science* **2004**, *303*, 1849−1851.
(64) López, R.; Rico, J. F.; Ramírez, G.; Ema, I.; Zorrilla, D.; Gadre, S. R.; Gadre, S. R. Topology of molecular electron density and electrostatic potential with DAMQT. *Comput. Phys. Commun.* **2017**, *214*, 207−215.

https://doi.org/10.1021/acsomega.3c00422
ACS Omega 2023, 8, 13993−14004